

Wave propagation in unbounded elastic domains using the spectral element method: formulation

Kristel C. Meza Fajardo^{*1} and Apostolos S. Papageorgiou²

¹*Departamento de Ingeniería Civil Universidad Nacional Autónoma de Honduras (UNAH), Tegucigalpa, Honduras*

²*Department of Civil Engineering, University of Patras, GR-26500 Patras, Greece*

(Received August 4, 2011, Revised January 25, 2011, Accepted April 10, 2012)

Abstract. The objective of the present paper is to review and implement the most recent developments in the Spectral Element Method (SEM), as well as improve aspects of its implementation in the study of wave propagation by numerical simulation in elastic unbounded domains. The classical formulation of the method is reviewed, and the construction of the mass matrix, stiffness matrix and the external force vector is expressed in terms of matrix operations that are familiar to earthquake engineers. To account for the radiation condition at the external boundaries of the domain, a new absorbing boundary condition, based on the Perfectly Matched Layer (PML) is proposed and implemented. The new formulation, referred to as the Multi-Axial Perfectly Matched Layer (M-PML), results from generalizing the classical Perfectly Matched Layer to a medium in which damping profiles are specified in more than one direction.

Keywords: elastic wave propagation; spectral element method; perfectly matched layer; engineering seismology

1. Introduction

Understanding the physics of earthquakes is a necessary step to assess their potential damage to man-made structures, and thus to develop efficient strategies for risk mitigation. Numerical simulations of the earthquake process have indeed become in the last two decades a major tool to improve such understanding. The development of computer technology, along with the wide availability of cost-effective equipment, has made it possible to solve numerically Partial Differential Equations (PDE) for which there are no known analytical solutions. In this context, the Spectral Element Method (SEM) has been recently adopted by the field of elastodynamics and is rapidly developing in order to address a wide variety of problems in the disciplines of global seismology and strong motion seismology. Originally developed to address problems in fluid dynamics, the SEM combines the flexibility of a Finite Element Method (FEM) with the accuracy of a spectral method, allowing the computation of accurate synthetic seismograms in heterogeneous earth models with arbitrary geometry. The SEM is a highly accurate numerical method and it is not cumbersome in dealing with non-flat free surface and spatially variable anelastic attenuation. One uses a weak formulation of the equations of motion, which are solved on a mesh of hexahedral elements that is

^{*}Corresponding author, Professor, E-mail: kristelmeza@unah.edu.hn

adapted to the geometry of the free surface as well as to that of the main internal discontinuities/interfaces of the model. The wavefield on the elements is discretized using high-degree Lagrange interpolants, and integration over an element is accomplished using the Gauss-Lobatto-Legendre (GLL) integration rule. This ensures *minimal* numerical grid *dispersion* and *anisotropy*. The most important property of the SEM is that the mass matrix is *exactly diagonal* by construction, which drastically simplifies the implementation and reduces the computational cost because one can use an *explicit* time integration scheme without matrix inversion. Furthermore, it allows for an efficient parallel implementation on a digital computer.

The name ‘Spectral Element Method’ originates from two previously developed numerical techniques for solving PDE on which it is based, namely, Pseudo-Spectral Methods and the Finite Element Method (FEM). Pseudo-spectral methods are known for their high accuracy and low memory requirements. However, their implementation in irregular geometries is limited because the position of the interpolation points is fixed, specified by the choice of basis-functions. On the other hand, the FEM has been widely adopted as a numerical tool for most applications since it has the advantage of being highly flexible when dealing with complex geometries. However, in simulations of seismic wave propagation, the accuracy of FEM is not satisfactory while that of the SEM is far superior (e.g. Padovani *et al.* 1994, Seriani and Priolo 1994, Seriani and Oliveira 2008).

The SEM was first introduced by Patera (1984) to solve problems of computational fluid dynamics. Its development was the result of combining the accuracy and rapid convergence of the pseudo-spectral methods with the geometrical flexibility of the FEM. Chebyshev polynomials were the basis polynomials for interpolation in the original work by Patera (1984). This choice was motivated by the fact that expansions with Chebyshev polynomials have the same (exponential) convergence as Fourier series. Hence, the word ‘*spectral*’ in the SEM is related to the exponential convergence it achieves when the order of interpolating polynomials is increased. The SEM with Chebyshev polynomials was successfully implemented to solve 1-D wave propagation problems (Priolo and Seriani 1991), and also in applications for 2-D and 3-D geological structures (Seriani and Priolo 1994, Priolo *et al.* 1994 Priolo 1999).

An alternative to the Chebyshev SEM was developed by Maday and Patera (1989), with the use of a Lagrange interpolation in conjunction with the GLL quadrature, leading to a *diagonal* structure of the mass matrix. Adopting such approach, Komatitsch (1997) and Komatitsch and Vilotte (1998) applied the SEM to simulate wave propagation in large-scale 3-D structures. Exploiting the advantage of an exactly diagonal mass matrix, they implemented an *explicit* time scheme and achieved an effective parallel implementation. Further extensions of the SEM have been developed for the use of 2-D triangular elements (Komatitsch *et al.* 2001) and non-conforming meshes (Chaljub 2000, Chaljub *et al.* 2003). The potential of SEM as an effective tool to address seismological problems has been illustrated by its successful applications in strong motion seismology (e.g. Komatitsch and Tromp 1999) and fault rupture dynamics (e.g. Ampuero 2002). Informative reviews of the SEM may be found in Komatitsch *et al.* (2005) and Chaljub *et al.* (2007).

For simulations related to wave propagation in unbounded domains, truncation of the domain is necessary, due to finite computational resources. An artificial boundary limiting the *computational* (or *physical*) domain is then introduced, and appropriate boundary conditions must be specified so that the solution in the physical domain is an accurate representation of the solution in the unbounded domain. It turns out that devising such boundary conditions is by no means a trivial matter. In recent years the ‘Perfectly Matched Layer’ (PML) has become the preferred absorbing

boundary for the elastic wave equation, due to its superior efficiency and flexibility when compared to other conditions. The PML was introduced by Bérenger (1994) as a material boundary condition for wave propagation problems in electromagnetism. The technique consists of surrounding the physical domain of interest with an absorbing layer of finite width such that all outgoing waves are damped out irrespective of their frequency and direction of propagation. The main feature of the PML is that, in the case of the continuum (i.e., before discretization) it does not introduce reflections at the interface between the layer and the physical medium (i.e., it is “*perfectly matched*”), although a small reflection is always present after discretization. Being a material absorbing condition, the PML leads naturally to sparse systems, it is well suited for implementation in parallel computers, and consequently, very attractive for numerical simulations. Despite the general success of the PML in most applications, there were still instances for which the performance of the PML did not meet expectations. In the case of elastic waves in isotropic media, it has been reported (Festa *et al.* 2005, Komatitsch and Martin 2007) that large reflections are obtained for waves entering the PML at grazing incidence and also that instabilities appear in long (in time) simulations. In addition, Bécache *et al.* (2003) documented that exponentially growing solutions could appear in some models for anisotropic media. All these problems were addressed and explained *mathematically* by Meza-Fajardo and Papageorgiou (2008, 2009, see also Meza-Fajardo 2007) who introduced a generalization of the original/classical PML, referred to as the M-PML. The ‘**M**’ stands for ‘**M**ulti-axial’ and is alluding to the fact that M-PML introduces damping profiles in more than one direction (as compared to the classical PML that introduces damping in only one direction). The M-PML makes possible the construction of stable and effective PML terminations, that can be used with confidence, for any kind of medium and source of excitation; in fact it has already been adopted in various applications (e.g. Bielak *et al.* 2010, Li and Bou-Matar 2010).

In the present work, the weak formulation of the Spectral Element Method for elastodynamics is presented in a tutorial fashion. The construction of the mass matrix, stiffness matrix and force vector is expressed in terms of matrix operations that are familiar to earthquake engineers. This is followed by a discussion of the algorithm that is adopted to follow in time the evolution of the solution of the *semi-discrete form* of the equation of motion (discretized over the spatial variables). The presentation is by necessity condensed due to space limitations. More details may be found in the doctoral thesis of the first author (Meza-Fajardo 2007). Although various aspects of the presentation that follows can be found in other presentations of the SEM (e.g. Komatitsch and Tromp 1999, Festa and Vilotte 2005), our presentation is comprehensive and detailed enough for the uninitiated to be able to follow and apply the method.

2. Statement of the problem – equation of motion

The *displacement* formulation of the elastodynamic initial value problem for a linear elastic solid is defined by (1) Cauchy’s equation of motion (also referred to as *momentum equation*), (2) generalized Hooke’s law and (3) initial conditions

$$\left. \begin{aligned} \rho \ddot{\mathbf{u}} &= \nabla \cdot \mathbf{T} + \mathbf{f} \\ \mathbf{T} &= \mathbf{C} : \nabla \mathbf{u} \\ \mathbf{u}_0(\mathbf{x}) &= \mathbf{u}(\mathbf{x}, 0) \quad \dot{\mathbf{u}}_0(\mathbf{x}) = \dot{\mathbf{u}}(\mathbf{x}, 0) \end{aligned} \right\} \Rightarrow \left\{ \begin{aligned} \rho \ddot{\mathbf{u}} &= \nabla \cdot [\mathbf{C} : \nabla \mathbf{u}] + \mathbf{f} \\ \mathbf{u}_0(\mathbf{x}) &= \mathbf{u}(\mathbf{x}, 0) \quad \dot{\mathbf{u}}_0(\mathbf{x}) = \dot{\mathbf{u}}(\mathbf{x}, 0) \end{aligned} \right. \quad (1)$$

where: $\mathbf{u}(\mathbf{x}, t)$ is the displacement vector field as a function of position \mathbf{x} and time t ; $\mathbf{T}(\mathbf{x}, t)$ is the stress tensor; $\mathbf{C}(\mathbf{x}, t)$ is the 4th order elasticity tensor; $\rho(\mathbf{x})$ is the mass density; $\mathbf{f}(\mathbf{x}, t)$ is the generalized body-force vector.

The above system of equations admits plane wave solutions of the form

$$\mathbf{u} = \mathbf{A} \exp[-i(\mathbf{k} \cdot \mathbf{x} - \omega t)] \quad (2)$$

where, \mathbf{A} is the *polarization vector*, $i = \sqrt{-1}$, and ω is the circular frequency. The vector $\mathbf{k} = [k_x, k_y, k_z]$, known as the *wave vector*, gives the direction of propagation of the wave front. Its amplitude $k = |\mathbf{k}| = \sqrt{k_x^2 + k_y^2 + k_z^2}$ is known as the *wave number*.

In the above formulation, seismic sources may be represented by *equivalent* body forces (e.g. Aki and Richards 1980, 2002)

$$\mathbf{f} = -\nabla \cdot \mathbf{m} \quad (3)$$

where, \mathbf{m} is the moment density tensor. For a point source acting at position \mathbf{x}_S , the moment density tensor can be expressed as

$$\mathbf{m} = \mathcal{M} \delta(\mathbf{x} - \mathbf{x}_S) S(t) \quad (4)$$

where, $\mathcal{M} = M_{ij} \mathbf{e}_i \mathbf{e}_j$ is the *moment tensor* expressed as a *dyadic* (Brand 1947, Simmonds 1994, Malvern 1969, Ben-Menahem and Singh 1981, 2000), M_{ij} are its components and $\mathbf{e}_i (i = x, y, z)$ are unit vectors along the x_i axes; $S(t)$ is the *source time function*; $\delta(\mathbf{x} - \mathbf{x}_S)$ denotes the Dirac Delta distribution indicating that the point source is concentrated at \mathbf{x}_S . Therefore, the body-force equivalent for a general seismic source is given by

$$\mathbf{f} = -M_{ij} \mathbf{e}_i \mathbf{e}_j S(t) \cdot \nabla \delta(\mathbf{x} - \mathbf{x}_S) = -M_{ij} \mathbf{e}_i \mathbf{e}_j S(t) \cdot \frac{\partial \delta(\mathbf{x} - \mathbf{x}_S)}{\partial x_k} \mathbf{e}_k = -M_{ij} S(t) \frac{\partial \delta(\mathbf{x} - \mathbf{x}_S)}{\partial x_j} \mathbf{e}_i \quad (5)$$

In particular, the moment tensor for a *point shear dislocation* is $\mathcal{M} = M_0(\mathbf{v}\mathbf{n} + \mathbf{n}\mathbf{v})$ and the corresponding body-force equivalent is given by the following expression

$$\mathbf{f} = -M_0(\mathbf{v}\mathbf{n} + \mathbf{n}\mathbf{v}) S(t) \cdot \nabla \delta(\mathbf{x} - \mathbf{x}_S) \quad (6)$$

where, M_0 the (scalar) *seismic moment*, \mathbf{v} is the unit vector defining the *direction of slip*, and \mathbf{n} is the unit vector *normal to the plane of slip* (no fault opening is assumed, i.e., $\mathbf{n} \cdot \mathbf{v} = 0$). For a point shear dislocation of infinitesimal area $d\Sigma$, with slip ΔU , embedded in an homogeneous isotropic elastic medium of rigidity μ , the seismic moment is given by

$$M_0 = \mu(\Delta U)(d\Sigma) \quad (7)$$

For a point shear dislocation, the moment tensor components M_{ij} in Eq. (5) may be expressed in terms of the *dip* δ , *rake* λ and *strike* ϕ_S of the fault plane (see Box 4.4 in Aki and Richards 1980, 2002).

Finally, the equivalent body-force for a *center of compression* or *explosion* is represented by dipoles of the same strength that are acting along three mutually perpendicular directions. The orientation of the dipoles is not important as long as they are of the same strength. Mathematically it is expressed as follows

$$\mathbf{f} = -M_0 \mathbf{e}_i \mathbf{e}_i S(t) \cdot \nabla \delta(\mathbf{x} - \mathbf{x}_S) = -M_0 \mathcal{J} S(t) \cdot \nabla \delta(\mathbf{x} - \mathbf{x}_S) = -M_0 S(t) \frac{\partial \delta(\mathbf{x} - \mathbf{x}_S)}{\partial x_i} \mathbf{e}_i \quad (8)$$

where, \mathcal{J} is the *unit dyadic* or the *idemfactor* [i.e., the complete dyadic (i.e., tensor) that transforms every vector \mathbf{a} into itself; the rectangular Cartesian components of the unit dyadic are represented by the identity matrix].

3. The weak form

In order to discretize the equation of motion using the SEM, we employ the weak (integral) form. We start by multiplying Cauchy's equation of motion by a time-independent generic *weighting function* (variation) $\mathbf{w}(\mathbf{x})$, and then the product is integrated over the spatial domain Ω of the problem

$$\int_{\Omega} \mathbf{w} \cdot \rho \frac{\partial^2 \mathbf{u}}{\partial t^2} d\Omega = \int_{\Omega} \mathbf{w} \cdot (\nabla \cdot \mathbf{T}) d\Omega + \int_{\Omega} \mathbf{w} \cdot \mathbf{f} d\Omega \quad (9)$$

The *strong* (differential) and *weak* (integral) forms are equivalent since Eq. (9) holds for any vector \mathbf{w} . Now, we make use of the following tensor identity (Drew 1961)

$$\nabla \cdot (\mathbf{T} \cdot \mathbf{w}) = (\nabla \cdot \mathbf{T}) \cdot \mathbf{w} + \tilde{\mathbf{T}} : \nabla \mathbf{w} \quad (10)$$

where the tilde “ \sim ” denotes “*transpose*”. For the stress tensor \mathbf{T} , indicating the operation of transposition, does not make any difference because it is *symmetric*. The above identity is applied to the first term on the right hand side (RHS) of Eq. (9)

$$\int_{\Omega} \mathbf{w} \cdot (\nabla \cdot \mathbf{T}) d\Omega = \int_{\Omega} [\nabla \cdot (\mathbf{T} \cdot \mathbf{w}) - \tilde{\mathbf{T}} : \nabla \mathbf{w}] d\Omega \quad (11)$$

The next step involves the application of the *divergence theorem* which is mathematically expressed as

$$\int_{\Omega} \nabla \cdot (\mathbf{T} \cdot \mathbf{w}) d\Omega = \int_{\Gamma} (\mathbf{T} \cdot \mathbf{w}) \cdot \mathbf{n} d\Gamma \quad (12)$$

where \mathbf{n} is a unit vector in the direction of the outward normal to the volume's boundary surface $\Gamma \equiv \partial\Omega$. The divergence theorem is a conservation law, which states that the net flux of a vector field inside a volume, (i.e., the volume integral of the divergence of the field), is equal to the net flow across the boundary enclosing the volume. From Eqs. (11) and (12) we obtain the result

$$\int_{\Omega} \mathbf{w} \cdot (\nabla \cdot \mathbf{T}) d\Omega = \int_{\Gamma} (\mathbf{T} \cdot \mathbf{w}) \cdot \mathbf{n} d\Gamma - \int_{\Omega} \tilde{\mathbf{T}} : \nabla \mathbf{w} d\Omega \quad (13)$$

Therefore, Eq. (9) takes the following form

$$\int_{\Omega} \mathbf{w} \cdot \rho \frac{\partial^2 \mathbf{u}}{\partial t^2} d\Omega = \int_{\Gamma} (\mathbf{T} \cdot \mathbf{w}) \cdot \mathbf{n} d\Gamma - \int_{\Omega} \tilde{\mathbf{T}} : \nabla \mathbf{w} d\Omega + \int_{\Omega} \mathbf{w} \cdot \mathbf{f} d\Omega \quad (14)$$

that may be expressed also in terms of the *traction vector* \mathbf{t} as follows

$$\int_{\Omega} \mathbf{w} \cdot \rho \frac{\partial^2 \mathbf{u}}{\partial t^2} d\Omega = \int_{\Gamma} \mathbf{w} \cdot \mathbf{t} d\Gamma - \int_{\Omega} \tilde{\mathbf{T}} : \nabla \mathbf{w} d\Omega + \int_{\Omega} \mathbf{w} \cdot \mathbf{f} d\Omega \quad (15)$$

Note that a *traction-free* boundary condition is automatically imposed by setting the first term on the RHS of the above equation equal to zero. This is one of the advantageous features of the weak formulation: the traction-free boundary condition is naturally satisfied, that is, it does not have to be imposed explicitly. On the other hand, since Eq. (15) is 2nd – order (in time) equation, the system is usually solved by expressing it as a 1st – order (in time) system in terms of velocities and displacements as follows

$$\int_{\Omega} \mathbf{w} \cdot \rho \dot{\mathbf{v}} d\Omega = - \int_{\Omega} \nabla \mathbf{w} : \tilde{\mathbf{T}}(\mathbf{u}) d\Omega + \int_{\Omega} \mathbf{w} \cdot \mathbf{f} d\Omega \quad (16)$$

$$\int_{\Omega} \mathbf{w} \cdot \dot{\mathbf{u}} d\Omega = \int_{\Omega} \mathbf{w} \cdot \mathbf{v} d\Omega \quad (17)$$

with initial conditions given in Eq. (1). In the above variational formulation, both displacements $\mathbf{u}(\mathbf{x}, t)$ and velocities $\mathbf{v}(\mathbf{x}, t) \equiv \dot{\mathbf{u}}(\mathbf{x}, t)$ are explicitly approximated as *primary* variables, while stresses are not fundamental unknowns and are derived from the discretization of the equation of motion, as the notation $\tilde{\mathbf{T}}(\mathbf{u})$ indicates. The admissible kinematic vector fields, displacement and velocity, defined on Ω , are assumed to be square integrable and to have square integrable first-order partial derivatives in space, over the domain Ω . Formally, $\mathbf{w}, \mathbf{u}, \mathbf{v} \in H^1(\Omega)$ (Hughes 1987). As pointed out by Festa and Vilotte (2005), physically, the above (*primal*) variational formulation can be directly derived from *Hamilton's extremum principle* [the system evolves along the trajectory that renders stationary (extremizes) the *action function*, i.e., the time integral of the Lagrangian] and represents the *perturbation* of the Lagrangian itself.

4. Spatial discretization

4.1 Domain decomposition and coordinate transformation

A set of rectangular Cartesian axes (x, y, z) is selected and the physical domain is divided into N_e non-overlapping elements. Then the integrals of the weak form are evaluated separately for every element domain Ω_e

$$\int_{\Omega_e} \mathbf{w} \cdot \rho \frac{\partial^2 \mathbf{u}}{\partial t^2} d\Omega_e \quad \int_{\Omega_e} \nabla \mathbf{w} : \tilde{\mathbf{T}}(\mathbf{u}) d\Omega_e \quad \int_{\Omega_e} \mathbf{w} \cdot \mathbf{f} d\Omega_e \quad (18)$$

To form a mesh over a general region the elements must be allowed to take general shapes. For 3-D problems, the discretization using the SEM is restricted to hexahedral elements. In the case of 2-D problems, the elements are quadrilateral. The sides of the 3-D hexahedral elements as well as the 2-D quadrilateral elements are *isomorphous* to the square. Hence, there exists a unique mapping from the square to each quadrilateral element. The reference or parent element is defined in terms of coordinates

$$-1 \leq \xi \leq 1 \quad -1 \leq \eta \leq 1 \quad -1 \leq \zeta \leq 1 \quad (19)$$

which are referred to as the *local* or *natural* coordinates. The parent element of simple geometric shape is then mapped into distorted shapes in the global Cartesian coordinate system. The mapping is defined in terms of a set of *shape functions* $N_a(\xi, \eta, \zeta)$, and a set of n_a *control* or *anchor nodes* $\mathbf{x}_a = \mathbf{x}(\xi_a, \eta_a, \zeta_a)$, $a = 1, 2, \dots, n_a$, which define the geometry of the element. Points on the two domains (i.e., the parent and physical domains) are then related as follows

$$x(\xi, \eta, \zeta) = \sum_{a=1}^{n_a} N_a(\xi, \eta, \zeta) x_a \quad y(\xi, \eta, \zeta) = \sum_{a=1}^{n_a} N_a(\xi, \eta, \zeta) y_a \quad z(\xi, \eta, \zeta) = \sum_{a=1}^{n_a} N_a(\xi, \eta, \zeta) z_a \quad (20)$$

The shape functions are n_d -products of *Lagrange polynomials* of degree one or two (for details see e.g. Hughes 1987), depending on the selected number of anchors nodes. The parameter n_d is the number of dimensions considered in the problem.

Evaluation of integrals Eq. (18) involves not only the shape functions but also their derivatives with respect to the global coordinates (x, y, z) . Evaluation of the integrals needs to be performed over the element area or volume. The derivatives in integrals Eq. (18) are easily converted from one coordinate system to another by means of the chain rule of partial differentiation, best expressed in matrix form by

$$\begin{pmatrix} \partial_{\xi}(\cdot) \\ \partial_{\eta}(\cdot) \\ \partial_{\zeta}(\cdot) \end{pmatrix} = \begin{bmatrix} \partial_{\xi}(x) & \partial_{\xi}(y) & \partial_{\xi}(z) \\ \partial_{\eta}(x) & \partial_{\eta}(y) & \partial_{\eta}(z) \\ \partial_{\zeta}(x) & \partial_{\zeta}(y) & \partial_{\zeta}(z) \end{bmatrix} \begin{pmatrix} \partial_x(\cdot) \\ \partial_y(\cdot) \\ \partial_z(\cdot) \end{pmatrix} = \mathbf{J} \begin{pmatrix} \partial_x(\cdot) \\ \partial_y(\cdot) \\ \partial_z(\cdot) \end{pmatrix} \quad (21)$$

The determinant J of matrix \mathbf{J} is referred to as the *Jacobian* and is used in the transformed integrals as follows

$$\iiint dx \, dy \, dz = \iiint J d\xi \, d\eta \, d\zeta \quad (22)$$

It is straightforward to compute the elements of matrix \mathbf{J} in terms of derivatives of the shape functions, i.e., $\partial_{\xi} N_a(\xi, \eta, \zeta)$, $\partial_{\eta} N_a(\xi, \eta, \zeta)$, $\partial_{\zeta} N_a(\xi, \eta, \zeta)$, and the coordinates of the anchor points (x_a, y_a, z_a) of the element (e.g. Hughes 1987).

4.2 Interpolation and integration of field variables over the elements

Numerical integration and interpolation are very closely related because one obvious method of integration is to fit a polynomial P_N of degree N to the integrand and then integrate the interpolant P_N . Since it is possible to exactly integrate the interpolant, then the error comes entirely from the difference between the integrand and P_N (Boyd 2000). It can be demonstrated (Boyd 2000) that the interpolant P_N that minimizes the interpolation error belongs to the family of Chebyshev polynomials. Because an expansion in terms of Chebyshev polynomials is related through a change of variable to a Fourier Cosine expansion, the convergence theory of Fourier series is practically transmitted to Chebyshev series. It is due to this spectral convergence of the Chebyshev polynomials that the term “spectral element” was coined and the early works on the SEM implemented those polynomials for interpolation of functions on elements (Patera 1984, Priolo and Seriani 1991, 1994). However, in later applications (Komatitsch 1997, Faccioli *et al.* 1997, Komatitsch and Vilotte 1998), a more convenient polynomial expansion that also retains spectral convergence was used. This alternative polynomial expansion is based on Lagrange interpolation with Legendre-Lobatto control points (Hildebrand 1956, 1987). The advantage of such interpolation is that, together with a discrete Gaussian integration rule, it leads to a mass matrix that is diagonal by construction. As a result, the SEM can be used with fully explicit time marching schemes, and therefore, an efficient implementation on parallel distributed memory architectures can be achieved.

4.2.1 Interpolation of field variables

As illustrated in the previous section, the shape of the boundary and volume elements can be defined in terms of low-degree Lagrange polynomials. In a traditional FEM, low-degree polynomials are also used as basis-functions for the representation of fields on the elements. In a SEM, on the other hand, a higher-degree Lagrange interpolant is used to express functions on the elements. Therefore, spectral elements are *subparametric*, because the interpolant used to describe the geometry is of lower order than the interpolant used to define the field variable.

A scalar function f on a parent element Ω_e is interpolated by products of Lagrange polynomials of degree N as (Lagrange Interpolation Formula for 3D)

$$f(\mathbf{x}(\xi, \eta, \zeta)) \cong P_N(\xi, \eta, \zeta) = \sum_{i,j,k=0}^N \ell_i(\xi)\ell_j(\eta)\ell_k(\zeta)f^{ijk} \quad (23)$$

where

$$f^{ijk} = f(\mathbf{x}(\xi_i, \eta_j, \zeta_k)) \quad (24)$$

and the functions $\ell_i(\xi)$, $\ell_j(\eta)$ and $\ell_k(\zeta)$, known as cardinal functions [or fundamental polynomials, Lagrange basis (or shape) functions], are polynomials of degree N defined by

$$\ell_i(x) \stackrel{\text{def}}{=} \prod_{j=0, j \neq i}^N \frac{x-x_j}{x_i-x_j} = \frac{(x-x_0)\cdots(x-x_{i-1})(x-x_{i+1})\cdots(x-x_N)}{(x_i-x_0)\cdots(x_i-x_{i-1})(x_i-x_{i+1})\cdots(x_i-x_N)} \quad (25)$$

The cardinal functions satisfy the condition

$$l_i(\xi_j) = \delta_{ij} \tag{26}$$

where δ_{ij} is the Kronecker Delta. Because of this property, the approximation of the functions inside the element is exact at the interpolation points. In a SEM the control points $\xi_i, i = 0, \dots, N$, needed in the definition of the Lagrange polynomials of degree N are selected to be the $(N + 1)$ Gauss-Lobatto-Legendre (GLL) points, which are the roots of the following equation

$$(1 - \xi^2) \frac{dL_N(\xi)}{d\xi} = 0 \tag{27}$$

where L_N denotes the Legendre polynomial of degree N . One can demonstrate that, for $N \geq 2$, Eq. (27) has $N + 1$ different real roots in the interval $[-1, +1]$, the first and the last ones being $\xi_0 = -1$ and $\xi_N = +1$ (Schwab 1998). Therefore, in a SEM some points always lie exactly on the boundaries of the elements. This choice of interpolation points is convenient because it allows one to enforce continuity of field variables across the element boundaries. For wave propagation problems using a SEM one typically uses a polynomial degree N between 5 and 10 to represent a function on the element (Komatitsch and Vilotte 1998).

The GLL points can be easily computed by numerical resolution (e.g. Newton-Raphson) (Canuto *et al.* 1988). The GLL points are not equally spaced in the interval $[-1, +1]$, but they are closer and closer moving toward the boundaries of the interval. Fig. 1 illustrates the nine Lagrange polynomials of degree eight based upon the nine Gauss-Lobatto-Legendre points defined by Eq. (27).

A convenient *vectorial* representation of the values of the field variable f at the GLL points is given by (e.g. Deville *et al.* 2002)

$$\begin{aligned} \mathbf{f} &= [f^1 \ f^2 \ \dots \ f^r \ \dots \ f^N] \\ &= [f^{000} \ f^{100} \ \dots \ f^{ijk} \ \dots \ f^{NNN}] \end{aligned} \tag{28}$$

where $\mathcal{N} = (N + 1)^3$ is the total number of nodal values in an element and the mapping

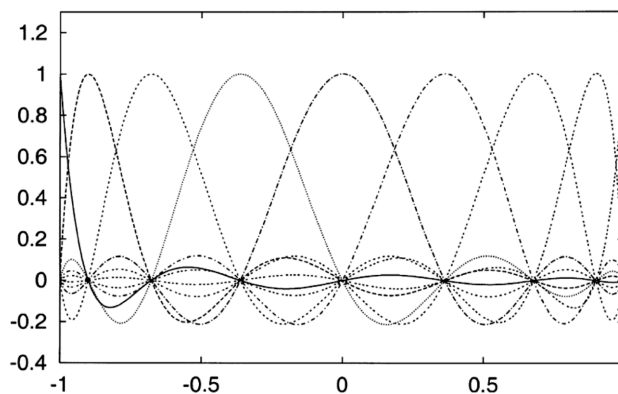


Fig. 1 Lagrange interpolants of degree $N=8$ at the Gauss-Lobatto-Legendre points (from Komatitsch and Tromp 1999, see also Deville *et al.* 2002)

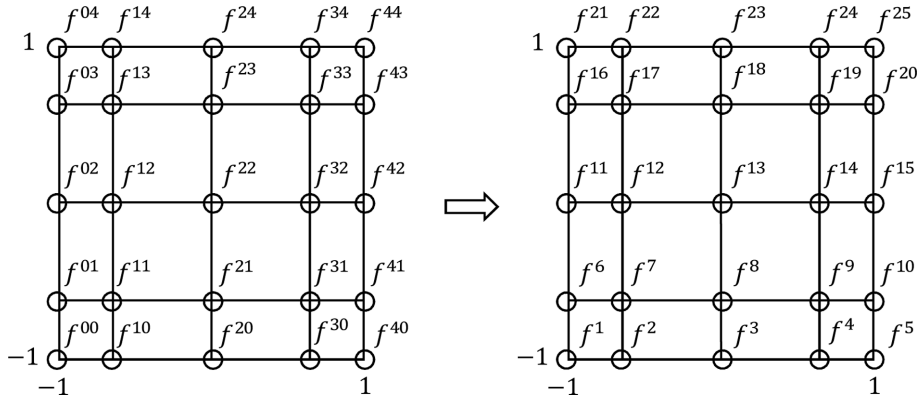


Fig. 2 Index mapping to translate the two-index coefficient representation to standard vector form

$$m = 1 + i + (N + 1)j + (N + 1)^2k \tag{29}$$

translates the three-index coefficient representation f^{ijk} to standard vector form f^m , with the first index advancing more rapidly. To illustrate the index mapping, the configuration for a 2-D parent element with interpolants of degree four is given in Fig. 2.

4.2.2 Approximation of derivatives

The derivatives of a field variable f with respect to the variables ξ , η and ζ , are approximated by applying differentiation in interpolation formula. Eq. (23). The values of the derivatives at the GLL points $\mathbf{x}(\xi_r, \eta_s, \zeta_t)$, with $r, s, t = 0, 1, \dots, N$ are given by

$$\frac{\partial f(\mathbf{x}(\xi_r, \eta_s, \zeta_t))}{\partial \xi} = \sum_{i,j,k=0}^N \frac{\partial \ell_i(\xi)}{\partial \xi} \Big|_{\xi_r} \ell_j(\eta_s) \ell_k(\zeta_t) f^{ijk} = \sum_{i=0}^N \frac{\partial \ell_i(\xi)}{\partial \xi} \Big|_{\xi_r} f^{ist} \tag{30}$$

$$\frac{\partial f(\mathbf{x}(\xi_r, \eta_s, \zeta_t))}{\partial \eta} = \sum_{i,j,k=0}^N \ell_i(\xi_r) \frac{\partial \ell_j(\eta)}{\partial \eta} \Big|_{\eta_s} \ell_k(\zeta_t) f^{ijk} = \sum_{j=0}^N \frac{\partial \ell_j(\eta)}{\partial \eta} \Big|_{\eta_s} f^{rjt} \tag{31}$$

$$\frac{\partial f(\mathbf{x}(\xi_r, \eta_s, \zeta_t))}{\partial \zeta} = \sum_{i,j,k=0}^N \ell_i(\xi_r) \ell_j(\eta_s) \frac{\partial \ell_k(\zeta)}{\partial \zeta} \Big|_{\zeta_t} f^{ijk} = \sum_{k=0}^N \frac{\partial \ell_k(\zeta)}{\partial \zeta} \Big|_{\zeta_t} f^{rst} \tag{32}$$

where property Eq. (26) has been used. The derivatives of the Legendre polynomials evaluated at the GLL points, appearing on the right hand side of Eqs. (30)-(32), are elements of the $(N + 1) \times (N + 1)$ one-dimensional derivative matrix

$$\mathbf{D} = [D_{pq}] = \left[\frac{d\ell_q(\xi)}{d\xi} \Big|_{\xi=\xi_p} \right] \tag{33}$$

The columns of the matrix correspond to the derivatives of the $(N + 1)$ polynomials, whereas the

rows correspond to the $(N + 1)$ GLL points. The calculation of the first derivatives of the Lagrange polynomials may be simply done with a subroutine provided by Funaro (1993). In this routine the derivatives Eq. (33), which are also known as (Legendre) collocation derivatives, are obtained by applying the following formula (see Funaro 1993, Deville *et al.* 2002)

$$D_{pq} = \left. \frac{d\ell_q(\xi)}{d\xi} \right|_{\xi=\xi_p} = \begin{cases} -\frac{1}{4}N(N+1) & p = q = 0 \\ \frac{L_N(\xi_p)}{L_N(\xi_q)} \frac{1}{\xi_p - \xi_q} & p \neq q \\ 0 & 1 \leq p = q \leq N-1 \\ \frac{1}{4}N(N+1) & p = q = N \end{cases} \quad (34)$$

Revisiting the derivatives of the field variable f , it becomes apparent that derivative Eq. (30) is the product of the r -th row of matrix \mathbf{D} with each vector $[f^{0st} f^{1st} \dots f^{Nst}]$, $s, t = 0, 1, \dots, N$. Similarly, evaluation of Eq. (31) involves multiplication of the s -th row of the collocation matrix \mathbf{D} with each vector $[f^{r0t} f^{r1t} \dots f^{rNt}]$. Finally, the derivative Eq. (32) is the result of the multiplication of the t -th row of matrix \mathbf{D} with each vector $[f^{rs0} f^{rs1} \dots f^{rsN}]$.

Considering again the vectorial representation of f given in Eq. (28), the operations described above may be expressed effectively by making use of tensor-product forms (e.g. Meyer 2000). Orszag (1980) pointed out early on that tensor-product forms were the foundation for efficient implementation of spectral methods. Expressions Eqs. (30)-(32) can be then written in the following form

$$\left\{ \frac{\partial f}{\partial \xi} \right\}_{\{\xi\}} \cong \mathbf{D}_\xi \mathbf{f} \quad \left\{ \frac{\partial f}{\partial \eta} \right\}_{\{\xi\}} \cong \mathbf{D}_\eta \mathbf{f} \quad \left\{ \frac{\partial f}{\partial \zeta} \right\}_{\{\xi\}} \cong \mathbf{D}_\zeta \mathbf{f} \quad (35)$$

the subscript $\{\xi\}$ denotes all the GLL points, and

$$\mathbf{D}_\xi = \mathbf{I}_{(N+1)} \otimes \mathbf{I}_{(N+1)} \otimes \mathbf{D} \quad \mathbf{D}_\eta = \mathbf{I}_{(N+1)} \otimes \mathbf{D} \otimes \mathbf{I}_{(N+1)} \quad \mathbf{D}_\zeta = \mathbf{D} \otimes \mathbf{I}_{(N+1)} \otimes \mathbf{I}_{(N+1)} \quad (36)$$

where $\mathbf{I}_{(N+1)}$ is the $(N + 1)$ identity matrix and \otimes denotes the tensor product. Furthermore, for consistency, the sequence with which the GLL points appear in vectors Eq. (35), must be exactly the same sequence they follow in vector \mathbf{f} given in Eq. (28).

4.2.3 Integration of field variables

As integrals Eq. (18) are separately evaluated for each element, the integration is performed over the parent domain using the so-called Gauss-Lobatto-Legendre quadrature rule

$$\int_{\Omega_e} f(\mathbf{x}) d\Omega_e(\mathbf{x}) = \int_{-1}^{+1} \int_{-1}^{+1} \int_{-1}^{+1} f(\xi, \eta, \zeta) J(\xi, \eta, \zeta) d\xi d\eta d\zeta \cong \sum_{i,j,k=0}^N \omega_i \omega_j \omega_k f^{ijk} J^{ijk} \quad (37)$$

where $\omega_i, i = 0, 1, \dots, N$ denote the weights of the GLL quadrature and

$$J^{ijk} = J(\xi_i, \eta_j, \zeta_k) \tag{38}$$

is the determinant of the Jacobian evaluated at the element GLL points. The GLL quadrature is a Gaussian integration rule whose collocation points are the $(N + 1)$ roots of the equation given in Eq. (27). The weights $\{\omega_i\}$ of the GLL quadrature are computed from the simple expressions (Abramowitz and Stegun 1972)

$$\omega_i = \begin{cases} \frac{2}{n(n+1)[L_n(\xi_i)]^2}, & \xi_i \neq \pm 1 \\ \frac{2}{n(n+1)}, & \xi_i = \pm 1 \end{cases} \tag{39}$$

As noted by Komatitsch and Tromp (1999), the GLL quadrature rule is exact only for polynomials of degree $(2N - 1)$. Thus, integration over parent or reference elements is never exact, since it involves the product of two polynomials of degree N : the field variable and the test function. However, the use of the GLL quadrature is attractive because it leads to a diagonal mass matrix, as it will be shown in the following section.

4.3 The element mass matrix

The element mass matrix is obtained from the integral

$$\int_{\Omega_e} \mathbf{w} \cdot \rho \frac{\partial^2 \mathbf{u}}{\partial t^2} d\Omega_e = \int_{-1}^{+1} \int_{-1}^{+1} \int_{-1}^{+1} \rho \frac{\partial^2 u_d(\xi, \eta, \zeta)}{\partial t^2} w_d(\xi, \eta, \zeta) J(\xi, \eta, \zeta) d\xi d\eta d\zeta \tag{40}$$

where $d = x, y, z$. Each displacement component u_d and test function w_d is approximated using Lagrange interpolation as it was detailed in section 4.2.1. Substitution of the interpolated field variables and test functions in Eq. (40) and application of the GLL integration rule leads to

$$\begin{aligned} \int_{\Omega_e} \mathbf{w} \cdot \rho \frac{\partial^2 \mathbf{u}}{\partial t^2} d\Omega_e &\cong \\ \sum_{i,j,k=0}^N \omega_i \omega_j \omega_k J^{ijk} \rho^{ijk} &\left\{ \sum_{r,s,t=0}^N \ell_r(\xi_i) \ell_s(\eta_j) \ell_t(\zeta_k) \frac{\partial^2 u_d^{rst}}{\partial t^2} \left[\sum_{m,p,q=0}^N \ell_m(\xi_i) \ell_p(\eta_j) \ell_q(\zeta_k) w_d^{mpq} \right] \right\} \tag{41} \\ &= \sum_{i,j,k=0}^N \omega_i \omega_j \omega_k J^{ijk} \rho^{ijk} \left(\frac{\partial^2 u_d^{ijk}}{\partial t^2} \right) w_d^{ijk} \end{aligned}$$

where the property Eq. (26) for the cardinal functions has been used. It is evident then that each component of acceleration at each degree of freedom is multiplied by the factor $\omega_i \omega_j \omega_k J^{ijk} \rho^{ijk}$ implying that the mass matrix is diagonal by construction. The fact that the mass matrix in the SEM is diagonal is a highly desirable property because it allows for a very significant reduction in the complexity and cost of the algorithm that is used to march the system in time.

$$\mathbf{C} = \begin{bmatrix} c_{11} & c_{16} & c_{15} & c_{16} & c_{12} & c_{14} & c_{15} & c_{14} & c_{13} \\ c_{61} & c_{66} & c_{65} & c_{66} & c_{62} & c_{64} & c_{65} & c_{64} & c_{63} \\ c_{51} & c_{56} & c_{55} & c_{56} & c_{52} & c_{54} & c_{55} & c_{54} & c_{53} \\ c_{61} & c_{66} & c_{65} & c_{66} & c_{62} & c_{64} & c_{65} & c_{64} & c_{63} \\ c_{21} & c_{26} & c_{25} & c_{26} & c_{22} & c_{24} & c_{25} & c_{24} & c_{23} \\ c_{41} & c_{46} & c_{45} & c_{46} & c_{42} & c_{44} & c_{45} & c_{44} & c_{43} \\ c_{51} & c_{56} & c_{55} & c_{56} & c_{52} & c_{54} & c_{55} & c_{54} & c_{53} \\ c_{41} & c_{46} & c_{45} & c_{46} & c_{42} & c_{44} & c_{45} & c_{44} & c_{43} \\ c_{31} & c_{36} & c_{35} & c_{36} & c_{32} & c_{34} & c_{35} & c_{34} & c_{33} \end{bmatrix} \quad (48)$$

The corresponding symmetric \mathbf{C} matrix for an isotropic elastic material will then be given by

$$\mathbf{C} = \begin{bmatrix} \lambda + 2\mu & 0 & 0 & 0 & \lambda & 0 & 0 & 0 & \lambda \\ 0 & \mu & 0 & \mu & 0 & 0 & 0 & 0 & 0 \\ 0 & 0 & \mu & 0 & 0 & 0 & \mu & 0 & 0 \\ 0 & \mu & 0 & \mu & 0 & 0 & 0 & 0 & 0 \\ \lambda & 0 & 0 & 0 & \lambda + 2\mu & 0 & 0 & 0 & \lambda \\ 0 & 0 & 0 & 0 & 0 & \mu & 0 & \mu & 0 \\ 0 & 0 & \mu & 0 & 0 & 0 & \mu & 0 & 0 \\ 0 & 0 & 0 & 0 & 0 & \mu & 0 & \mu & 0 \\ \lambda & 0 & 0 & 0 & \lambda & 0 & 0 & 0 & \lambda + 2\mu \end{bmatrix} \quad (49)$$

If the derivatives of the test functions are organized in a vector form ($\partial_{\mathbf{x}}\mathbf{w}$) that has the same structure as the vector of displacement derivatives ($\partial_{\mathbf{x}}\mathbf{u}$) in Eq. (46), the inner product $\int_{\Omega_e} \nabla \mathbf{w} : \mathbf{T} d\Omega_e$ becomes

$$\int_{\Omega_e} \nabla \mathbf{w} : \mathbf{T} d\Omega_e = \int_{\Omega_e} (\partial_{\mathbf{x}}\mathbf{w})^T \mathbf{C} (\partial_{\mathbf{x}}\mathbf{u}) d\Omega_e \quad (50)$$

Now, because the integration over the element is performed in the parent domain, as follows

$$\int_{\Omega_e} \nabla \mathbf{w} : \mathbf{T} d\Omega_e \cong \int_{-1}^{+1} \int_{-1}^{+1} \int_{-1}^{+1} [(\partial_{\mathbf{x}}\mathbf{w}(\xi, \eta, \zeta))]^T \mathbf{C}(\xi, \eta, \zeta) [\partial_{\mathbf{x}}\mathbf{u}(\xi, \eta, \zeta)] J(\xi, \eta, \zeta) d\xi d\eta d\zeta \quad (51)$$

the inverse of matrix \mathbf{J} is needed to transform the derivatives, since it easily follows from Eq. (21) that $\partial_{\mathbf{x}}(\cdot) = \mathbf{J}^{-1} \partial_{\xi}(\cdot)$.

Let us then note that vector Eq. (46) can be expressed as

$$\partial_{\mathbf{x}}\mathbf{u} = \tilde{\mathbf{D}}_{\mathbf{x}}\mathbf{u} \quad (52)$$

$$\tilde{\mathbf{D}}_{\mathbf{x}} = \begin{bmatrix} \partial_x & \partial_y & \partial_z & & & & & & \\ & & & \partial_x & \partial_y & \partial_z & & & \\ & & & & & & \partial_x & \partial_y & \partial_z \end{bmatrix}^T \quad \mathbf{u} = \begin{pmatrix} u_x \\ u_y \\ u_z \end{pmatrix} \quad (53)$$

$$\mathcal{J}^e = \begin{bmatrix} \mathcal{J}_{\xi,x} & \mathcal{J}_{\eta,x} & \mathcal{J}_{\zeta,x} \\ \mathcal{J}_{\xi,y} & \mathcal{J}_{\eta,y} & \mathcal{J}_{\zeta,y} \\ \mathcal{J}_{\xi,z} & \mathcal{J}_{\eta,z} & \mathcal{J}_{\zeta,z} \end{bmatrix}_{(3\mathcal{N}) \times (3\mathcal{N})} \quad (60)$$

Therefore, Eq. (56) can be simply expressed as

$$\int_{\Omega_e} \nabla \mathbf{w} : \mathbf{T} d\Omega_e \cong \mathbf{W}^{eT} \hat{\mathbf{D}}_{\mathbf{x}}^T (\mathbf{I}_9 \otimes \Omega) \hat{\mathbf{C}}^e \hat{\mathbf{D}}_{\mathbf{x}} \mathbf{U}^e \quad (61)$$

where

$$\hat{\mathbf{D}}_{\mathbf{x}} = (\mathbf{I}_3 \otimes \mathcal{J}^e) \hat{\mathbf{D}}_{\xi} \quad (62)$$

while, $\hat{\mathbf{D}}_{\xi}$ is a $9\mathcal{N} \times 3\mathcal{N}$ matrix and \mathbf{U}^e is a $3\mathcal{N}$ vector, given by

$$\hat{\mathbf{D}}_{\xi} = \begin{bmatrix} \mathbf{D}_{\xi} & \mathbf{D}_{\eta} & \mathbf{D}_{\zeta} & \mathbf{0} & \mathbf{0} & \mathbf{0} & \mathbf{0} & \mathbf{0} & \mathbf{0} \\ \mathbf{0} & \mathbf{0} & \mathbf{0} & \mathbf{D}_{\xi} & \mathbf{D}_{\eta} & \mathbf{D}_{\zeta} & \mathbf{0} & \mathbf{0} & \mathbf{0} \\ \mathbf{0} & \mathbf{0} & \mathbf{0} & \mathbf{0} & \mathbf{0} & \mathbf{0} & \mathbf{D}_{\xi} & \mathbf{D}_{\eta} & \mathbf{D}_{\zeta} \end{bmatrix}^T \quad \mathbf{U}^e = \begin{pmatrix} \mathbf{u}_x \\ \mathbf{u}_y \\ \mathbf{u}_z \end{pmatrix} \quad (63)$$

Using the above notation, the element stiffness matrix \mathbf{K}^e , may be expressed as follows

$$\mathbf{K}^e = \hat{\mathbf{D}}_{\mathbf{x}}^T (\mathbf{I}_9 \otimes \Omega) \hat{\mathbf{C}}^e \hat{\mathbf{D}}_{\mathbf{x}} \quad (64)$$

Furthermore, by virtue of property Eq. (A3) from the Appendix, the product $(\mathbf{I}_9 \otimes \Omega)(\mathbf{C} \otimes \mathbf{I}_{\mathcal{N}})$ is equal to $(\mathbf{C} \otimes \Omega)$ and thus Eq. (64) reduces to a simpler form

$$\mathbf{K}^e = \hat{\mathbf{D}}_{\mathbf{x}}^T (\mathbf{C} \otimes \Omega) \hat{\mathbf{D}}_{\mathbf{x}} \quad (65)$$

Now, since the elastic coefficient matrix \mathbf{C} is symmetric and matrix Ω is diagonal (thus also symmetric), property Eq. (A7) in the Appendix indicates that $(\mathbf{C} \otimes \Omega)^T = \mathbf{C}^T \otimes \Omega^T = \mathbf{C} \otimes \Omega$. Consequently the stiffness matrix given in Eq. (65) is symmetric.

Once the nodal displacements of the element are determined, the internal force vector $\mathbf{F}^{int,e}$ can then be computed as

$$\mathbf{F}^{int,e} = \mathbf{K}^e \mathbf{U}^e \quad (66)$$

It should be remarked that the classical formulation of the stiffness matrix using the symmetric strain tensor can be alternatively used. The stiffness matrix is formulated here in terms of the displacement gradient for convenience, since this is the form needed to discretize the equations for the absorbing boundary condition with the SEM.

4.5 The element external force vector

With the equivalent body force Eq. (3) the external force term in the weak form of the equation of motion becomes

$$\int_{\Omega} \mathbf{w} \cdot \mathbf{f} d\Omega = - \int_{\Omega} \mathbf{w} \cdot (\nabla \cdot \mathbf{m}) d\Omega \quad (67)$$

Applying tensor identity Eq. (10) and the divergence theorem Eq. (12) on the RHS of Eq. (67), we obtain the source term for slip on a finite fault plane Σ

$$\int_{\Omega} \mathbf{w} \cdot \mathbf{f} d\Omega = \int_{\Sigma} \nabla \mathbf{w} : \mathbf{m} d\Sigma \quad (68)$$

For a point source acting at \mathbf{x}_S , substitution of Eq. (4) in the RHS of Eq. (68) and evaluation of the integral (using the properties of the Dirac Delta function) gives

$$\int_{\Omega} \mathbf{w} \cdot \mathbf{f} d\Omega = S(t) \mathcal{M} : \nabla \mathbf{w}(\mathbf{x}_S) \quad (69)$$

Parenthetically we point out that the same result may be obtained by substituting for f the expression of Eq. (5).

If the point source is located at one of the GLL points of an element, the RHS of Eq. (69) can be computed using the vectorial representation for the values of the test functions at the element nodes \mathbf{W}^e given in Eq. (57). As usual, for computations we express the moment tensor and gradient of test functions tensor in vector form

$$S(t) \mathcal{M} : \nabla \mathbf{w}(\mathbf{x}_S) = S(t) \partial_{\mathbf{x}} \mathbf{w}^T \Big|_{\mathbf{x}_S} \tilde{\mathcal{M}} \quad (70)$$

where

$$\tilde{\mathcal{M}} = \left[M_{xx} \ M_{xy} \ M_{xz} \ M_{yx} \ M_{yy} \ M_{yz} \ M_{zx} \ M_{zy} \ M_{zz} \right]^T \quad (71)$$

The vector $\partial_{\mathbf{x}} \mathbf{w}^T \Big|_{\mathbf{x}_S}$ is in turn expressed as

$$\partial_{\mathbf{x}} \mathbf{w}^T \Big|_{\mathbf{x}_S} = (\mathbf{I}_3 \otimes \mathbf{J}_S^{-1}) \hat{\mathbf{D}}_S \mathbf{W}^e \quad (72)$$

where \mathbf{J}_S^{-1} is the 3×3 inverse of the \mathbf{J} matrix, evaluated at $\xi_S = (\xi_S, \eta_S, \zeta_S)$, the local coordinates corresponding the GLL point where the source is acting, namely

$$\mathbf{J}_S^{-1} = \begin{bmatrix} \partial_x \xi & \partial_x \eta & \partial_x \zeta \\ \partial_y \xi & \partial_y \eta & \partial_y \zeta \\ \partial_z \xi & \partial_z \eta & \partial_z \zeta \end{bmatrix}_{\xi_S} \quad (73)$$

and matrix $\hat{\mathbf{D}}_S$ is $9 \times 3\mathcal{N}$ block matrix given by

$$\hat{\mathbf{D}}_S = \begin{bmatrix} \mathbf{d}_{\xi_S} & \mathbf{d}_{\eta_S} & \mathbf{d}_{\zeta_S} & \mathbf{0} & \mathbf{0} & \mathbf{0} & \mathbf{0} & \mathbf{0} & \mathbf{0} \\ \mathbf{0} & \mathbf{0} & \mathbf{0} & \mathbf{d}_{\xi_S} & \mathbf{d}_{\eta_S} & \mathbf{d}_{\zeta_S} & \mathbf{0} & \mathbf{0} & \mathbf{0} \\ \mathbf{0} & \mathbf{0} & \mathbf{0} & \mathbf{0} & \mathbf{0} & \mathbf{0} & \mathbf{d}_{\xi_S} & \mathbf{d}_{\eta_S} & \mathbf{d}_{\zeta_S} \end{bmatrix}^T \quad (74)$$

Matrices \mathbf{d}_{ξ_S} , \mathbf{d}_{η_S} and \mathbf{d}_{ζ_S} , are row matrices of length \mathcal{N} , computed in the following manner

$$\begin{aligned} \mathbf{d}_{\xi_S} &= \mathbf{h}_{\xi_S} \otimes \mathbf{h}_{\xi_S} \otimes \mathbf{d}(\xi_S) \\ \mathbf{d}_{\eta_S} &= \mathbf{h}_{\eta_S} \otimes \mathbf{d}(\eta_S) \otimes \mathbf{h}_{\eta_S} \\ \mathbf{d}_{\zeta_S} &= \mathbf{d}(\zeta_S) \otimes \mathbf{h}_{\zeta_S} \otimes \mathbf{h}_{\zeta_S} \end{aligned} \quad (75)$$

where $\mathbf{d}(\xi_S)$, $\mathbf{d}(\eta_S)$ and $\mathbf{d}(\zeta_S)$ are the *rows* of the one-dimensional derivative matrix \mathbf{D} (Eq. (33)) corresponding to the ξ_S , η_S and ζ_S local coordinates, respectively. Finally, \mathbf{h}_{ξ_S} , \mathbf{h}_{η_S} and \mathbf{h}_{ζ_S} , are row vectors of length $(N+1)$ with only one non-zero entry, which also corresponds to the ξ_S , η_S and ζ_S coordinates, respectively.

4.6 Global mass matrix, internal and external force vectors

As stated in section 3, the discrete displacement field is sought in the space of vector fields on the domain Ω that are square integrable and have square-integrable first-order partial derivatives in space. Thus, inter-element continuity for the displacement field should be incorporated. As in classical FEM, continuity of a field across element interfaces is enforced by adding the corresponding entries of all elements that share nodes. Thus, if \mathbf{U} is the vector containing the values of the displacement field at the global nodes of the domain Ω , the assembly of the global mass matrix \mathbb{M} , internal force vector \mathbb{F}^{int} , and external force vector \mathbb{F}^{ext} can be symbolically written as

$$\mathbb{M} = \mathcal{A}_{e=1}^{n_e} \{\mathbf{M}^e\} \quad \mathbb{F}^{ext} = \mathcal{A}_{e=1}^{n_e} \{F^{ext,e}\} \quad \mathbb{F}^{int} = \mathcal{A}_{e=1}^{n_e} \{F^{int,e}\} \quad (76)$$

where \mathbf{M}^e , $F^{ext,e}$ and $F^{int,e}$ are the mass matrix, external force and internal force vectors, respectively, of the e -th element (in SEM, the mass matrix is diagonal, and thus can also be expressed as a vector). The assembling operation goes over the total number of elements n_e , adding the entries corresponding to the same global node. The global numbering counts only once those nodes that are shared by more than one element. The global numbering of the nodes is related to the local numbering (i.e., the numbering at the element level), through the connectivity matrix \mathcal{Q} . The element \mathcal{Q}_{je} of the connectivity matrix will then give the global node number corresponding to the j -th local node of the e -th element. It should be remarked at this stage that the assembly of the internal force vector is preferred, because for the large size of the problems in seismological applications, the assembly of the global stiffness matrix turns out to be a too costly operation. Finally, the semi-discrete form of the equation of motion is expressed by

$$\mathbb{M}\ddot{\mathbf{U}}(t) = \mathbb{F}^{ext}(t) - \mathbb{F}^{int}(\mathbf{U}(t)) \quad (77)$$

where the notation $\mathbb{F}^{int}(\mathbf{U}(t))$ indicates that the global internal force vector is computed from the displacement vector.

5. Stress-velocity formulation

The elastodynamic equations may be cast in a form of a symmetric first-order hyperbolic system, (subject to initial conditions of velocity and stress), where both stress and velocity fields are considered as primary variables

$$\begin{aligned}\rho\dot{\mathbf{v}} &= \nabla \cdot \mathbf{T} + \mathbf{f} \\ \dot{\mathbf{T}} &= \mathbf{C}:\nabla\mathbf{v} \\ \mathbf{v}(\mathbf{x}, 0) &= \mathbf{v}_0(\mathbf{x}) \quad \mathbf{T}(\mathbf{x}, 0) = \mathbf{T}_0(\mathbf{x})\end{aligned}\tag{78}$$

The weak form of this system is obtained by multiplying the equation of motion and the constitutive equation in Eq. (78) with time-independent test function $\mathbf{w}(\mathbf{x})$ and $\mathbf{S}(\mathbf{x})$, respectively, and integrating over the spatial domain Ω as follows

$$\int_{\Omega} \mathbf{w} \cdot \rho\dot{\mathbf{v}} d\Omega = \int_{\Omega} \mathbf{w} \cdot (\nabla \cdot \mathbf{T}) d\Omega + \int_{\Omega} \mathbf{w} \cdot \mathbf{f} d\Omega\tag{79}$$

$$\int_{\Omega} \mathbf{S}:\dot{\mathbf{T}} d\Omega = \int_{\Omega} \mathbf{S}:\mathbf{C}:\nabla\mathbf{v} d\Omega\tag{80}$$

After the usual integration by parts, application of the divergence theorem, and imposition of the stress-free surface boundary condition, the weak form of Eq. (78) becomes

$$\int_{\Omega} \mathbf{w} \cdot \rho\dot{\mathbf{v}} d\Omega = - \int_{\Omega} \mathbf{T}:\nabla\mathbf{w} d\Omega + \int_{\Omega} \mathbf{w} \cdot \mathbf{f} d\Omega\tag{81}$$

$$\int_{\Omega} \mathbf{S}:\dot{\mathbf{T}} d\Omega = \int_{\Omega} \mathbf{S}:\mathbf{C}:\nabla\mathbf{v} d\Omega\tag{82}$$

Now, in the classical velocity-stress formulation, the stresses \mathbf{T} and their variations \mathbf{S} are sought in the space of symmetric tensor fields that are square integrable over Ω , together with square integrable divergence. However, in the formulation adopted in this work, which was proposed by Festa and Villote (2005), the vector fields, test functions and velocity, \mathbf{w} , \mathbf{v} belong to the space $H^1(\Omega)$, while the stress field is symmetric and (only) square integrable. That is, the stress field \mathbf{T} and its variation \mathbf{S} belong to the space $L_2(\Omega)$. Thus, the stress space does not incorporate inter-element continuity. It can be demonstrated (Festa and Vilotte 2005) that, if the stresses are discretized making use of the same polynomial order and collocation points as the velocity, such a (spatial) discretization leads to the same system of algebraic equations as the one obtained from the primal formulation given by Eqs. (16) and (17). This equivalence allows the implementation of the displacement formulation in part of the domain and of the stress-velocity formulation in the remaining part. More specifically, based on the above observation, the absorbing layers can be discretized using the stress-velocity formulation, whereas the physical domain can be discretized using classical formulation in terms of velocities and displacements.

6. Time integration scheme

The semi-discrete form of the equation of motion (discretized over the spatial variables), after the global mass matrix, internal force and external force vectors have been assembled takes the form of Eq. (77). This 2nd-order system may be alternatively written as a 1st-order system in terms of velocity and displacement

$$\begin{Bmatrix} \dot{\mathbf{V}}(t) \\ \dot{\mathbf{U}}(t) \end{Bmatrix} = \begin{Bmatrix} \mathbf{M}^{-1}[\mathbf{F}^{ext}(t) - \mathbf{F}^{int}(\mathbf{U}(t))] \\ \mathbf{V}(t) \end{Bmatrix} \quad (83)$$

Let us adopt the following compact notation

$$\begin{aligned} \dot{\mathbf{y}}(t) &= \begin{Bmatrix} \dot{\mathbf{V}}(t) \\ \dot{\mathbf{U}}(t) \end{Bmatrix} = \begin{Bmatrix} \mathbf{M}^{-1}[\mathbf{F}^{ext}(t) - \mathbf{F}^{int}(\mathbf{U}(t))] \\ \mathbf{V}(t) \end{Bmatrix} = \mathbf{f}(\mathbf{y}, t) \\ \mathbf{y}(t) &= \begin{Bmatrix} \mathbf{V}(t) \\ \mathbf{U}(t) \end{Bmatrix}, \quad t \geq t_0, \quad \mathbf{y}(t) = \mathbf{y}_0 \end{aligned} \quad (84)$$

In what follows, the subscripts $(n-1)$, n and $(n+1)$ represent the approximants of the field variables at time stations $(t-\Delta t)$, t and $(t+\Delta t)$, respectively (e.g. $\mathbf{U}_{n-1} \cong \mathbf{U}(t-\Delta t)$, $\mathbf{U}_n \cong \mathbf{U}(t)$, $\mathbf{U}_{n+1} \cong \mathbf{U}(t+\Delta t)$, etc.).

A Newmark scheme could be implemented to describe the evolution of the above system. Such a scheme would be 2nd-order accurate and implicit. However, in order to exploit the advantage of the exact diagonal mass matrix of the SEM, an explicit time integration method is desired. For that purpose we consider the following alternative scheme based on the midpoint integration rule

$$\begin{aligned} \dot{\mathbf{y}}_{n+1} &= \mathbf{f}(\mathbf{y}_{n+1}, t_{n+1}) \\ \mathbf{y}_{n+1} &= \mathbf{y}_n + (\Delta t)\dot{\mathbf{y}}_{n+1/2} \end{aligned} \quad (85)$$

Shifting (backward) by half a time step of the top equation in Eq. (85) and applying the resulting time marching scheme to Eq. (84), we obtain

$$\begin{Bmatrix} \mathbf{V}_{n+1} - \mathbf{V}_n \\ \mathbf{U}_{n+1} - \mathbf{U}_n \end{Bmatrix} = (\Delta t) \begin{Bmatrix} \mathbf{M}^{-1}[\mathbf{F}_{n+1/2}^{ext} - \mathbf{F}^{int}(\mathbf{U}_{n+1/2})] \\ \mathbf{V}_{n+1/2} \end{Bmatrix} \quad (86)$$

By shifting (backward) by half a time step the lower equation in Eq. (86), we obtain the following staggered time grid

$$\begin{Bmatrix} \mathbf{V}_{n+1} - \mathbf{V}_n \\ \mathbf{U}_{n+1/2} - \mathbf{U}_{n-1/2} \end{Bmatrix} = (\Delta t) \begin{Bmatrix} \mathbf{M}^{-1}[\mathbf{F}_{n+1/2}^{ext} - \mathbf{F}^{int}(\mathbf{U}_{n+1/2})] \\ \mathbf{V}_n \end{Bmatrix} \quad (87)$$

It is with this time scheme, proposed by Festa and Vilotte (2005), that the implementation of the absorbing conditions (PML equations) can be performed without affecting the displacement formulation of the SEM in the physical domain (details of such implementation may be found in Meza-Fajardo 2007). On the other hand, it is interesting to note that the time integration scheme based on the midpoint rule, described above, is a particular case of the Generalized Method proposed by Modak and Sotelino (2002) for structural dynamics applications. According to the analysis of Generalized Method by Modak and Sotelino (2002), the time-marching scheme in Eq. (87) is 2nd-order accurate. Thus, even though the SEM exhibits high spatial accuracy, the overall accuracy of the simulations is governed by the time marching scheme.

Since the multi-step time-integration scheme is explicit, it is only conditionally stable, and the Courant-Friedrichs-Lewy (CFL) stability condition (Courant *et al.* 1928) must be satisfied. The CFL condition states that the speed at which information travels cannot exceed one grid cell per time step

$$v_{\max}(\Delta t) \sqrt{\frac{1}{(\Delta x)^2} + \frac{1}{(\Delta y)^2} + \frac{1}{(\Delta z)^2}} \leq 1 \quad (88)$$

where v_{\max} is the maximum wave speed (P -wave speed) and Δx , Δy and Δz are the minimum nodal distances of the spatial grid. For $\Delta x = \Delta y = \Delta z$ the above condition reduces to

$$v_{\max} \left(\frac{\Delta t}{\Delta x} \right) \leq \frac{1}{\sqrt{D}} = \frac{1}{\sqrt{3}} \cong 0.577 \quad (89)$$

where D is the dimension of the problem. Based on such an analysis Komatitsch and Vilotte (1998) propose that the CFL number $n_C \stackrel{\text{def}}{=} \max[v_{\max}(\Delta t/\Delta x)]$ should not exceed 0.6. The CFL condition limits the maximum possible time increment and therefore the efficiency of any explicit time-marching scheme. In addition, in a linear medium, the size of the time step can be correlated to the frequency content of the signal radiated by the source since the grid spacing must be selected so as to properly sample the high frequency content of the signal. If the time variation of the source is described by a Ricker wavelet (Ricker 1945) of the form

$$R(t) = [2\pi^2 f_0^2 (T-t_0)^2 - 1] \exp[-\pi^2 f_0^2 (T-t_0)^2] \quad (90)$$

where f_0 is the dominant frequency and t_0 is the onset time, the maximum frequency that needs to be accounted for is approximately $2.5f_0$ (e.g. Komatitsch and Tromp 1999). For $N = 5 - 10$, which are typical polynomial degrees used in SEM, the element size is chosen such that the average number of points per minimum wavelength in an element, is roughly equal to 5 (Seriani and Priolo 1994, Komatitsch 1997, Faccioli *et al.* 1997). The minimum wavelength is the one corresponding to the maximum frequency mentioned above.

7. Implementation of the M-PML absorbing boundary condition

Space limitations do not permit us to present the derivation of the variational form of the equations of the M-PML termination and the time-marching scheme that allows its efficient

implementation. A comprehensive treatment of this subject may be found in Meza-Fajardo (2007). The formulation of the equations over the domain of the PML terminations is not performed in terms of displacements because it would lead to third derivatives of displacements with respect to time or time convolutions. To avoid such undesirable developments, a stress-velocity formulation is adopted. The successful interface of the two formulations, the displacement formulation over the physical domain and that of stress-velocity over the PML terminations, is accomplished using the staggered time grid Eq. (87) presented in the previous section.

8. Demonstrative applications

We consider three rather simple examples to demonstrate the efficacy of the SEM in propagating the disturbance generated by a source without any visible (numerical) dispersion, and the effectiveness of the M-PML in absorbing the waves entering the artificial terminations surrounding the physical domain.

The first example, displayed in Fig. 3, shows the propagation of radiation of an embedded line explosive source through two isotropic half-spaces. Details of the physical domain properties and discretization parameters are listed in Table 1. It is worth pointing out the effectiveness of the M-PML in absorbing the incident waves, even though the source is located very close to two of the artificial terminations. Finally, once all the disturbances have moved away from the physical domain, no reflected disturbances remain, as it is evident from the snapshot at $t = 7.5$ s.

The second example, displayed in Fig. 4, shows again the disturbance generated by an explosive (line) source embedded in a 2-D medium composed of two isotropic layers on an isotropic half space and a stress-free (upper) boundary. The properties of the three media are detailed in Table 2. The formation of a Rayleigh wave is evident as a result of the interaction of the radiation emitted by the source with the free surface at the top. Also we can follow the propagation of the Rayleigh wave parallel to the free surface. We notice again the effectiveness of the M-PML in absorbing all

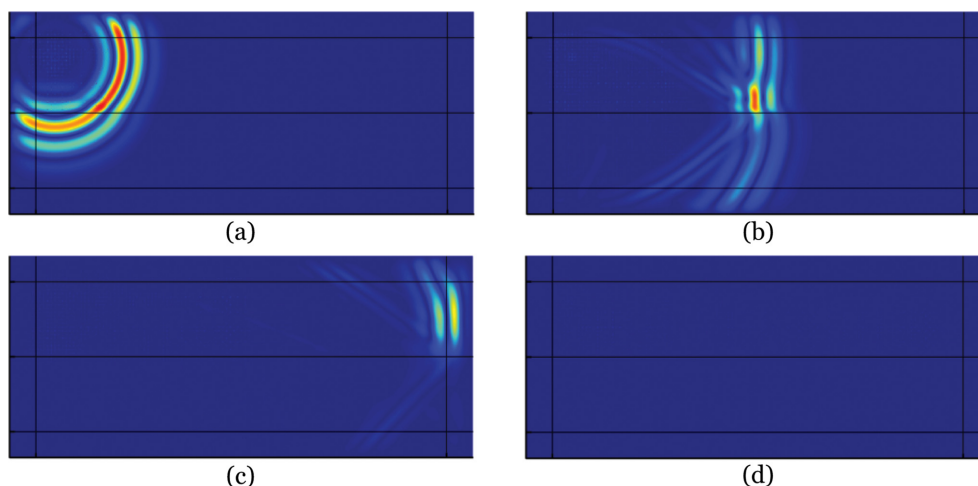


Fig. 3 Snapshots of propagation of velocity magnitude in two isotropic elastic half-spaces with M-PML terminations at (a) $t=1$ s, (b) $t=2$ s, (c) $t=3.8$ s and (d) $t=7.5$ s

Table 1 Properties and discretization parameters for simulation with two isotropic half-spaces

Upper half space dimensions		Source location	
Length	11 km	From left boundary	0.5 km
Width	2 km	From bottom boundary	3.5 km
Upper half space properties		Ricker wavelet parameters	
Density	$2.7E+12$ kg/km ³	Dominant frequency	2.5 Hz
S-wave velocity	1.87 km/s	Onset time	0.4 s
P-wave velocity	3.2 km/s	Discretization parameters	
Lower half space dimensions		Polynomial degree	8
Length	11 km	Element side	0.1 km
Width	2 km	Elements along PML width	7
Lower half space properties		Time step	0.00047 s
Density	$2.7E+12$ kg/km ³	Total duration	7.5 s
S-wave velocity	2.34 km/s		
P-wave velocity	4 km/s		

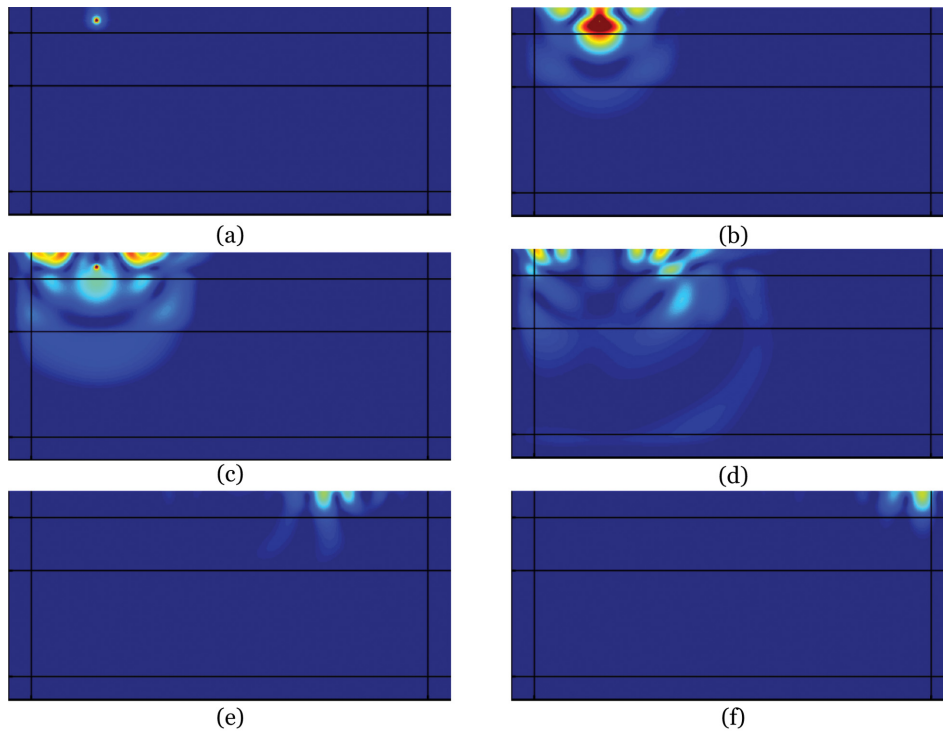


Fig. 4 Snapshots of propagation of velocity magnitude in two isotropic layers on an isotropic half-space and a stress-free (upper) boundary at (a) $t=1$ s, (b) $t=3$ s, (c) $t=4$ s, (d) $t=5$ s, (e) $t=15$ s and (f) $t=20$ s

types of incident waves, including the Rayleigh wave.

As a third example we examine the effectiveness of the SEM (with M-PML as absorbing boundary conditions) in simulating propagation of elastic waves in heterogeneous media. The

Table 2 Properties and discretization parameters for simulation with a layered medium

Upper layer dimensions		Source location	
Length	30 km	From left boundary	4.9 km
Width	2 km	From bottom boundary	12.9 km
Upper layer properties		Ricker wavelet parameters	
Density	$2.2E+12 \text{ kg/km}^3$	Dominant frequency	0.4 Hz
<i>S</i> -wave velocity	1.80 km/s	Onset time	2.5 s
<i>P</i> -wave velocity	3.2 km/s	Discretization parameters	
Middle layer dimensions		Polynomial degree	5
Length	30 km	Element side	0.25 km
Width	4 km	Elements along PML width	7
Middle layer properties		Time step	0.0012 s
Density	$2.25E+12 \text{ kg/km}^3$	Total duration	20 s
<i>S</i> -wave velocity	3 km/s		
<i>P</i> -wave velocity	5.4 km/s		
Lower half space dimensions			
Length	30 km		
Width	8 km		
Lower half space properties			
Density	$3.18E+12 \text{ kg/km}^3$		
<i>S</i> -wave velocity	4.3 km/s		
<i>P</i> -wave velocity	7.5 km/s		

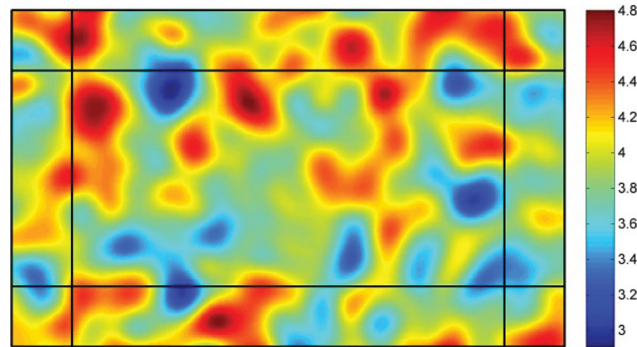


Fig. 5 Gaussian random field with fractional fluctuation $\varepsilon=0.10$, correlation length $a=0.2 \text{ km}$ and average velocity $\alpha_0=4 \text{ km/s}$. The random medium is generated for the physical domain and for the M-PML terminations as well

physical domain is 4 km long and 2 km wide. We consider again an explosive (line) source. Fig. 5 displays a realization of a Gaussian random field with fractional fluctuation $\varepsilon=0.10$, correlation length $a=0.2 \text{ km}$ and average velocity $\alpha_0=4 \text{ km/s}$ (for definitions of the above parameters see Sato and Fehler 1998). The same random distribution was used for the *S*-wave velocity with average $\beta_0=2.2818 \text{ km/s}$ and for the mass density with average $\rho_0=2.393 \times 10^{12} \text{ kg/km}^3$.

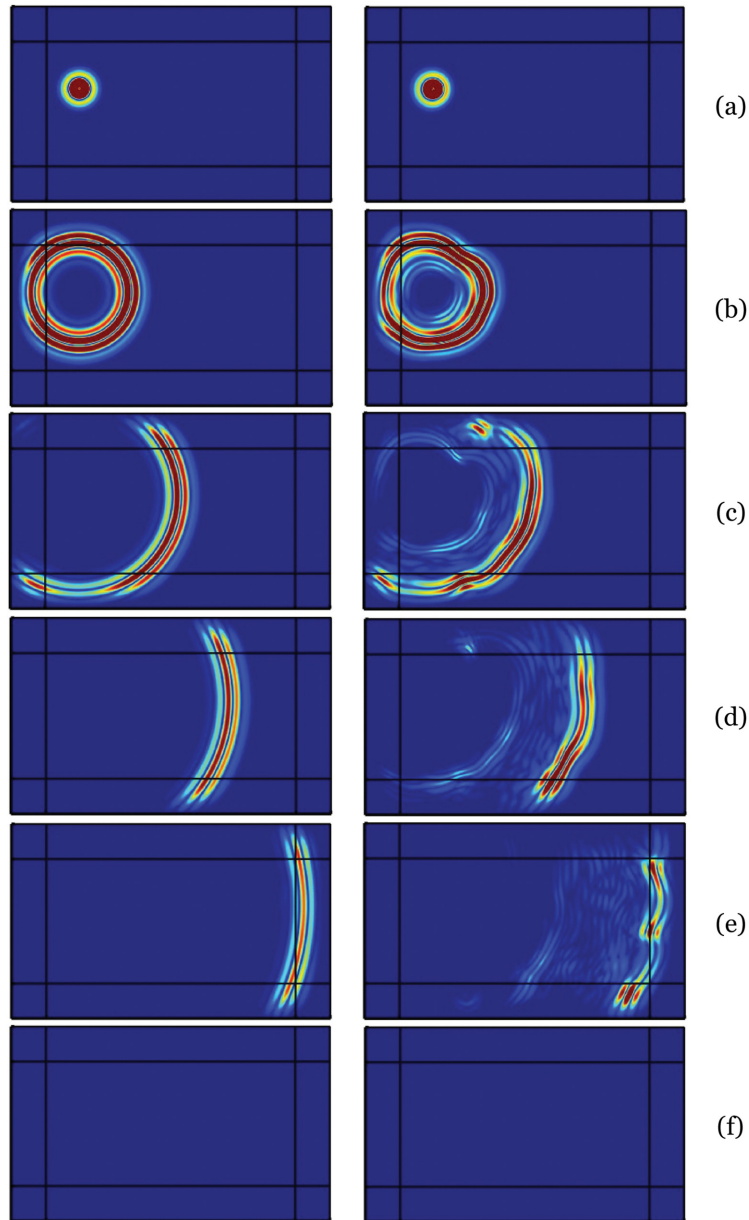


Fig. 6 Snapshots of propagation of velocity magnitude through the random medium (right column) and the corresponding homogeneous medium (left column) at (a) $t=0.01$ s, (b) $t=0.03$ s, (c) $t=0.05$ s, (d) $t=0.07$ s, (e) $t=1.0$ s and (f) $t=5.0$ s

Fig. 6 displays and compares snapshots of the response of the random medium (right column) with the response of the corresponding homogeneous medium (left column) at time-instants $t = 0.01, 0.03, 0.05, 0.07, 1.0$ and 5.0 s. Table 3 details the discretization parameters for the two media. Distortion of the wave front and appearance of coda, generated by scattering due to the velocity fluctuations of the medium, are clearly visible in the random medium.

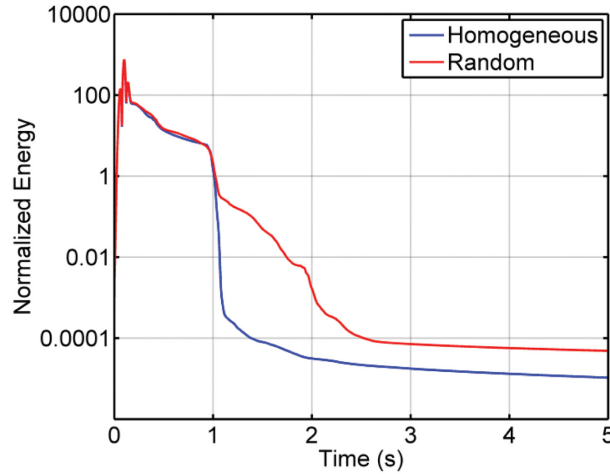


Fig. 7 Comparison of energy decay within the homogeneous and random media. The energy is normalized with respect to the value it attains in the homogeneous medium at $t = 1$ s

Table 3 Discretization parameters for simulation with heterogeneous and homogeneous media

Source location	
From left boundary	0.52 km
From bottom boundary	1.24 km
Ricker wavelet parameters	
Dominant frequency	10 Hz
Onset time	0.1 s
Discretization parameters	
Polynomial degree	8
Element side	0.08 km
Elements along PML width	7
Time step	0.00030 s
Total duration	5 s

Finally, Fig. 7 displays the evolution with time of (normalized) seismic energy present over the entire physical domain considered in the computation. As expected, for the random medium it takes longer for the seismic energy in the physical domain to be reduced to (practically) zero levels because of the presence of coda (scattered waves).

9. Conclusions

The Spectral Element Method (SEM) combined with the Multi-axial Perfectly Matched Layer (M-PML) (used as wave-absorbing terminations) constitutes a very effective, efficient and accurate method for elastic wave propagation. Its potential for applications in the discipline of Elastodynamics, in general, and Engineering Seismology, in particular, is evident.

References

- Abramowitz, M. and Stegun, I.A. (1972), *Handbook of mathematical functions with formulas, graphs and mathematical tables*, 9th printing, Dover, New York.
- Aki, K. and Richards, P.G. (2002), *Quantitative seismology, Second Edition*, University Science Books, California.
- Ampuero, J.P. (2002), *Etude physique et numerique de la nucleation des seismes*, PhD Thesis, Universite Paris 7, Paris, France.
- Bécache, E., Fauqueux, S. and Joly, P. (2003), “Stability of perfectly matched layers, group velocities and anisotropic waves”, *J. Comput. Phys.*, **188**(2), 399-433.
- Ben-Menahem, A. and Singh, S.J. (1998), *Seismic waves and sources*, Dover Publications, New York.
- Bérenger, J.P. (1994), “A perfectly matched layer for the absorption of electromagnetic waves”, *J. Comput. Phys.*, **114**(2), 185-200.
- Bielak, J., Graves, R.W., Olsen, K.B., Taborda, R., Ramirez-Guzman, L., Day, S.M., Ely, G.P., Roten, D., Jordan, T.H., Maechling, P.J., Urbanic, J., Cui, Y.F. and Juve, G. (2010), “The shakeOut earthquake scenario: Verification of three simulation sets”, *Geophys. J. Int.*, **180**(1), 375-404.
- Brand, L. (1947), *Vector and tensor analysis*, Wiley.
- Canuto, C., Hussaini, M.Y., Quarteroni, A. and Zang, T.A. (1988), *Spectral methods in fluid dynamics*, Springer-Verlag, New York.
- Chaljub, E. (2000), “Modélisation numérique de la propagation d’ondes sismiques en géométrie sphérique: application à la sismologie globale”, *PhD Thesis*, Université Paris VII Denis Diderot, Paris, France.
- Chaljub, E., Capdeville, Y. and Vilotte, J.P. (2003), “Solving elastodynamics in a fluid-solid heterogeneous sphere: a parallel spectral element approximation on non-conforming grids”, *J. Comput. Phys.*, **15**(6), 363-369.
- Chaljub, E., Komatitsch, D., Capdeville, Y., Vilotte, J.P., Valette, B. and Festa, G. (2007), “Spectral-element analysis in seismology”, *Adv. Geophys.*, **48**, 365-419.
- Courant, R., Friedrichs, K. and Lewy, H. (1928), “Über die partiellen differenzengleichungen der mathematischen physik”, *Math. Ann.*, **100**(1), 32-74.
- Deville, M.O., Fischer, P.F. and Mund, E.H. (2002), *High-order methods for incompressible fluid flow*, Cambridge University Press, Cambridge.
- Drew, T.B. (1961), *Handbook of vector and polyadic analysis*, Reinhold Publishing Co., New York.
- Faccioli, E., Maggio, F., Paolucci, R. and Quarteroni, A. (1997), “2D and 3D elastic wave propagation by a pseudospectral domain decomposition method”, *J. Seismol.*, **1**(3), 237-251.
- Festa, G. and Vilotte, J.P. (2005), “The newmark scheme as velocity-stress time staggering: an efficient PML implementation for spectral element simulations of elastodynamics”, *Geophys. J. Int.*, **161**(3), 798-812.
- Festa, G., Delavaud, E. and Vilotte, J.P. (2005), “Interaction between surface waves and absorbing boundaries for wave propagation in geological basins: 2D numerical simulations”, *Geophys. Res. Lett.*, **32**(L20306), doi:10.1029/2005GL024091.
- Funaro, D. (1993), *FORTRAN routines for spectral methods*, Istituto di Analisi Numerica, Pavia, Italy.
- Hildebrand, F.B. (1987), *Introduction to numerical analysis*, Second Edition, Dover Publications, New York, USA.
- Hughes, T.J.R. (1987), *The finite element method, linear static and dynamic finite element analysis*, Prentice Hall, Englewood Cliffs, NJ.
- Komatitsch, D. (1997), “Méthodes spectrales et elements spectraux pour l’équation de l’élastodynamique 2D et 3D en milieu hétérogène”, *PhD Thesis*, Institut de Physique du Globe, Paris, France.
- Komatitsch, D. and Vilotte, J.P. (1998), “The spectral element method”, *Geophys. J. Int.*, **154**, 146-153.
- Komatitsch, D. and Tromp, J. (1999), “Introduction to the spectral element method for three-dimensional seismic wave propagation”, *Geophys. J. Int.*, **139**(3), 806-822.
- Komatitsch, D. and Tromp, J. (2001), “Modelling of seismic wave propagation at the scale of the earth on a large Beowulf”, *Proceedings of the ACM/IEEE Supercomputing SC2001 Conference*.
- Komatitsch, D., Tsuboi, S. and Tromp, J. (2005), “The spectral-element method in seismology”, *Seismic Earth: Array Analysis of Broadband Seismograms*, **157**, 205-228.
- Komatitsch, D. and Martin, R. (2007), “An unsplit convolutional Perfectly Matched Layer improved at grazing

- incidence for the seismic wave equation”, *Geophysics*, **72**(5), 155-167.
- Li, Y.F. and Bou Matar, O. (2010), “Convolutional perfectly matched layer for elastic second-order wave equation”, *J. Acoust. Soc. Am.*, **127**(3), 1318-1327.
- Maday, Y. and Patera, A.T. (1989), “Spectral element methods for the incompressible Navier-Stokes equations”, *State of the art Surveys in Computational Mechanics*, ASME, New York, 71-143.
- Malvern, L.E. (1969), *Introduction to the mechanics of a continuous medium*, Prentice Hall.
- Meyer, C.D. (2000), *Matrix analysis and applied linear algebra*, SIAM, Philadelphia.
- Meza-Fajardo, K.C. (2007), “Numerical simulation of wave propagation in unbounded elastic domains using the spectral element method”, *European School for Reduction of Seismic Risk (ROSE School)*, University of Pavia, Italy.
- Meza-Fajardo, K.C. and Papageorgiou, A.S. (2008), “A non-convolutional split-field, perfectly matched layer for wave propagation in isotropic and anisotropic elastic media: stability analysis”, *B. Seismol. Soc. Am.*, **98**(4), 1811-1836.
- Meza-Fajardo, K.C. and Papageorgiou, A.S. (2010), “On the stability of a non-convolutional perfectly matched layer for isotropic elastic media”, *Soil Dyn. Earthq. Eng.*, **30**(3), 68-81.
- Modak, S. and Sotelino, E.D. (2002), “The generalized method for structural dynamics applications”, *Adv. Eng. Softw.*, **33**(7-10), 565-577.
- Orzag, S.A. (1980), “Spectral element methods for problems in complex geometries”, *J. Comput. Phys.*, **37**(1), 70-92.
- Padovani, E., Priolo, E. and Seriani, G. (1994), “Low- and high-order finite element method: Experience in seismic modeling”, *J. Comput. Acoust.*, **2**(4), 371-422.
- Patera, A.T. (1984), “A spectral element method for fluid dynamics: laminar flow in a channel expansion”, *J. Comput. Phys.*, **54**(3), 468-488.
- Priolo, E. and Seriani, G. (1991), “A numerical investigation of Chebyshev spectral element method for acoustic wave propagation”, *Proceedings of the 13th IMACS Conference on Computational Applied Mathematics*, Dublin, Ireland, **2**, 551-556.
- Priolo, E., Carcione, J.M. and Seriani, G. (1994), “Numerical simulation of interface waves by high-order spectral modelling techniques”, *J. Acoust. Soc. Am.*, **95**(2), 681-693.
- Priolo, E. (1999), “Earthquake ground motion simulation through the 2-D spectral element method”, *Proceedings of the International Conference on Computational Acoustics*, Trieste, Italy.
- Ricker, N. (1945), “The computation of output disturbances from amplifiers for true wavelet inputs”, *Geophysics*, **10**(2), 207-220.
- Sato, H. and Fehler, M. (1998), *Seismic wave propagation and scattering in the heterogeneous earth*, AIP Press/ Springer Verlag, New York.
- Schwab, C.H. (1998), *Up- and hp-finite element methods*, Oxford University Press, Oxford.
- Seriani, G. and Priolo, E. (1994), “Spectral element method for acoustic wave simulation in heterogeneous media”, *Finite Elem. Anal. Des.*, **16**(3-4), 337-348.
- Seriani, G. and Oliveira, S.P. (2008), “Dispersion analysis of spectral element methods for elastic wave propagation”, *Wave Motion*, **45**(6), 729-744.
- Simmonds, J.G. (1994), *A brief on tensor analysis*, Second Edition, Springer-Verlag.

Appendix: Tensor product and matrices

The tensor product (Kronecker product and direct product) of two matrices $\mathbf{A}_{m \times n}$ and $\mathbf{B}_{p \times q}$ is defined to be the $mp \times nq$ matrix (Meyer 2000)

$$\underbrace{\mathbf{A}}_{m \times n} \otimes \underbrace{\mathbf{B}}_{p \times q} = \begin{bmatrix} a_{11}\mathbf{B} & a_{12}\mathbf{B} & \cdots & a_{1n}\mathbf{B} \\ a_{21}\mathbf{B} & a_{22}\mathbf{B} & \cdots & a_{2n}\mathbf{B} \\ \vdots & \vdots & \ddots & \vdots \\ a_{m1}\mathbf{B} & a_{m2}\mathbf{B} & \cdots & a_{mn}\mathbf{B} \end{bmatrix}_{mp \times nq} \quad (\text{A1})$$

The elementary properties of the tensor product are listed below (conformability of the matrices is assumed)

$$\mathbf{A} \otimes (\mathbf{B} \otimes \mathbf{C}) = (\mathbf{A} \otimes \mathbf{B}) \otimes \mathbf{C} \quad (\text{A2})$$

$$(\mathbf{A} \otimes \mathbf{B})(\mathbf{C} \otimes \mathbf{D}) = \mathbf{AC} \otimes \mathbf{BD} \text{ (if } \mathbf{A} \mathbf{C} \text{ and } \mathbf{B} \mathbf{D} \text{ exist)} \quad (\text{A3})$$

$$(\mathbf{A} + \mathbf{B}) \otimes \mathbf{C} = (\mathbf{A} \otimes \mathbf{C}) + (\mathbf{B} \otimes \mathbf{C}) \quad (\text{A4})$$

$$\mathbf{A} \otimes (\mathbf{B} + \mathbf{C}) = (\mathbf{A} \otimes \mathbf{B}) + (\mathbf{A} \otimes \mathbf{C}) \quad (\text{A5})$$

$$(\mathbf{A} + \mathbf{B})^{-1} = \mathbf{A}^{-1} \otimes \mathbf{B}^{-1} \quad (\text{A6})$$

$$(\mathbf{A} \otimes \mathbf{B})^T = \mathbf{A}^T \otimes \mathbf{B}^T \quad (\text{A7})$$